



OPEN

SUBJECT AREAS:
OPTICAL MATERIALS
SOLAR CELLS
POLYMERS
PHOTONIC DEVICESVertical phase separation in bulk heterojunction solar cells formed by *in situ* polymerization of fullerideLipei Zhang¹, Xing Xing¹, Lingling Zheng¹, Zhijian Chen^{1,2}, Lixin Xiao^{1,2}, Bo Qu^{1,2} & Qihuang Gong¹¹State Key Laboratory for Mesoscopic Physics and Department of Physics, Peking University, Beijing 100871, China, ²New Display Device and System Integration Collaborative Innovation Center of the West Coast of the Taiwan Strait, Fuzhou 350002, China.Received
7 November 2013Accepted
1 May 2014Published
27 May 2014Correspondence and
requests for materials
should be addressed toZ.J.C. (zjchen@pku.
edu.cn); L.X.X.
(lxxiao@pku.edu.cn)
or Q.H.G. (qhong@
pku.edu.cn)

Vertical phase separation of the donor and the acceptor in organic bulk heterojunction solar cells is crucial to improve the exciton dissociation and charge transport efficiencies. This is because whilst the exciton diffusion length is limited, the organic film must be thick enough to absorb sufficient light. However, it is still a challenge to control the phase separation of a binary blend in a bulk heterojunction device architecture. Here we report the realization of vertical phase separation induced by *in situ* photo-polymerization of the acrylate-based fulleride. The power conversion efficiency of the devices with vertical phase separation increased by 20%. By optimising the device architecture, the power conversion efficiency of the single junction device reached 8.47%. We believe that *in situ* photo-polymerization of acrylate-based fulleride is a universal and controllable way to realise vertical phase separation in organic blends.

As the exciton diffusion length is limited and there is a difference in the mobility of the charge carriers^{1–4} through the organic film, an interpenetrating network structure of donor and acceptor materials is needed to assist in exciton separation and charge carrier transport in organic heterojunction solar cells^{5,6}. This requires the two materials to form a bicontinuous channel that can provide not only a large interface area between the electron donor and electron acceptor materials for efficient exciton dissociation, but also continuous pathways for more effective charge transport to the corresponding electrodes. This results in a reduction of the charge recombination and the space charge accumulation within the photoactive layer^{7–10}. It is believed that space charge accumulation decreases the photocurrent^{11–13}.

Conceptually, vertical phase separation (VPS) is where electron donor materials which allow hole transportation, gradually distribute towards the anode while the electron acceptor materials which allow electron transportation, gradually distribute towards the cathode. In other words, the vertical composition of the donor and the acceptor materials can affect the transport of charges to their respective electrodes after they are generated at the donor-acceptor interface of bulk heterojunction (BHJ)^{14–17}. Therefore, the charge recombination can be reduced. This would enhance the power conversion efficiency (PCE) and prevent degradation of the cell performance as the illumination time increases.

VPS can be achieved using various processes such as solvent additives^{18,19}, thermal annealing^{20–24}, vapour annealing^{25–30}, field induction^{31,32} and stepwise deposition³³. Although there are several approaches, it is still a challenge to achieve a real VPS in a universal and controllable way.

When ultraviolet (UV) light propagates through most organic materials, strong absorption creates a gradient in the UV intensity along the propagation direction^{34–36}. In polymerizable monomers, the rate of polymerization scales with the UV intensity along the propagation direction. In regions that have a stronger UV intensity, the polymerizable monomers are consumed faster, which results in a concentration difference of the monomers. This drives the diffusion of the monomers from the unpolymerized monomer-rich areas to the polymerized region. Thus a polymer gradient is created, along with a counter gradient of unpolymerized monomers^{34–36}.

In a bulk heterojunction structure, the conventional fullerene acceptors such as [6,6]-phenyl-C61 butyric acid methyl ester (PC₆₀BM), and [6,6]-phenyl-C71 butyric acid methyl ester (PC₇₀BM) tend to form discontinuous islands which are obstacles to electron transport. To avoid these discontinuous structures, we introduced an acrylate group to the fullerene acceptor by hydrolysing the PCBM and the esterification of the corresponding product with 4-hydroxybutyl acrylate (Fig. 1a). After the mixture of the acrylate-based fullerene and the donor was subjected to the above-mentioned UV polymerization method, donor and acceptor concentration gradients

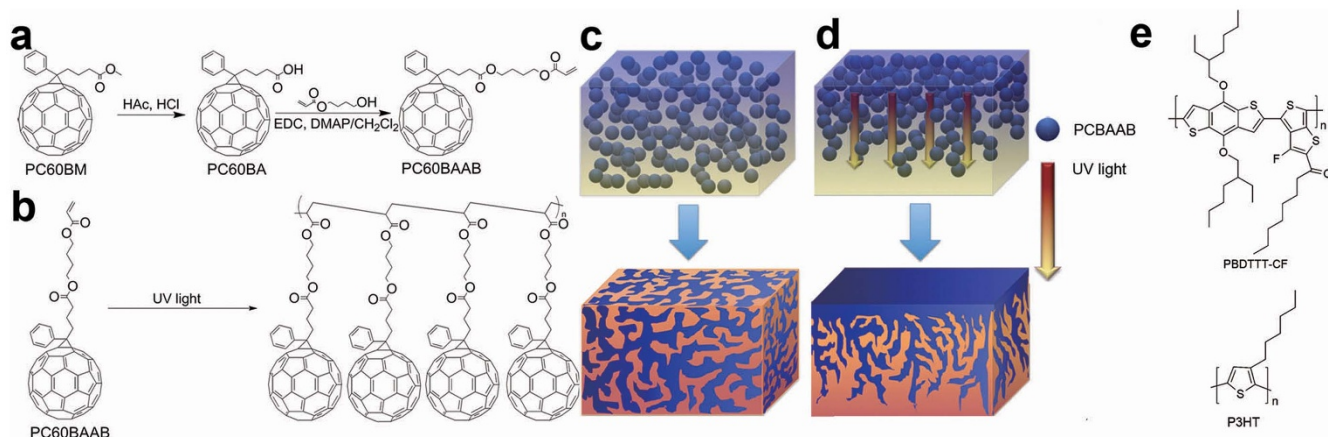


Figure 1 | (a) Synthesis of PC₆₀BAAB. The synthesis of PC₇₀BAAB follows the same route. (b) Photo-polymerization of PC₆₀BAAB. (c) The conventional BHI structure and the related phase separation that was formed by solvent annealing or thermal annealing. (d) When ultraviolet (UV) light propagates through the mixture, strong absorption creates a gradient of UV intensity along the propagation direction. The PCBAAB concentration gradient is formed during photo-polymerization. Thus vertical phase separation via *in situ* polymerization of PCBAAB occurs. The vertical phase separation aids charge transport and reduces charge accumulation. (e) The molecular structures of the donor materials.

form. Therefore, not only was the continuous acceptor structure formed, but also VPS was obtained (as shown in Fig. 1b and 1d, respectively).

In this work, poly(3-hexylthiophene-2,5-diyl) (P3HT) and poly[1-(6-{4,8-bis[(2-ethylhexyl)oxy]-6-methylbenzo[1,2-b:4,5-b']dithiophen-2-yl}-3-fluoro-4-methylthieno[3,4-b]thiophen-2-yl)-1-octanone] (PBDTTT-CF) were chosen as the donor materials, and the corresponding acrylate-based [6,6]-phenyl C61 butyric acid 4-hydroxybutyl acrylate ester (PC₆₀BAAB), [6,6]-phenyl C71 butyric acid 4-hydroxybutyl acrylate ester (PC₇₀BAAB) were chosen as acceptor materials for the devices. By changing the incident direction of the UV light, the direction of the donor and acceptor concentration gradients can be reversed to get either conventional or inverted devices. In conventional devices, the UV light is incident from the upper side of the active layer. For the inverted devices, the irradiation direction is reversed. The PCE of the devices with VPS, whether in the conventional or inverted device architecture, were improved with an enhancement of over 20% in comparison with the control devices without VPS. By further optimizing the architecture of the devices according to our earlier method³⁷, the PCE of the single-junction device reached 8.47%.

Results

***In situ* polymerization of PCBAAB.** For photo-polymerization of PCBAAB, the samples were irradiated using a weak UV light (0.1 mW/cm²). The intensity of the UV light controlled the polymerization speed to ensure that PCBAAB migrated through the whole film during photo-polymerization. To test the photo-polymerization of PCBAAB, the unpolymerized and polymerized active layer were measured using Fourier transform infrared spectroscopy (FTIR). As shown in Fig. 2, for the PBDTTT-CF:PC₇₀BAAB blend the peak at 1656 cm⁻¹ is attributed to absorption of the double bond of acrylate. Compared with the unpolymerized sample, the double bond absorption peak of the polymerized sample is weak, which confirms the *in situ* polymerization of PC₇₀BAAB.

VPS induced by *in situ* polymerization of PCBAAB. X-ray photo-emission spectroscopy (XPS) was performed to investigate the composition of the active layer at the top surfaces. This was achieved by inspecting the differences in XPS intensities of the carbon 1s and sulfur 2p bands. For P3HT:PC₆₀BAAB, the C 1s signal of the polymerized sample was extremely strong compared with that of the unpolymerized sample whereas the S 2p peak of the polymerized sample was weak, as shown in Fig. 3a. The fullerene PC₆₀BAAB is carbon rich,

while only P3HT contains sulfur. Thus, the PC₆₀BAAB concentration at the top surface of the polymerized sample is higher than that of the unpolymerized sample. Meanwhile, the top surface of the unpolymerized sample is P3HT rich. This confirms that the migration of the PC₆₀BAAB is in the opposite direction to the UV-light propagation.

Transmittance electron microscopy (TEM) was used to investigate the morphology of the donor/acceptor distribution. Figure 3b shows the cross-section of the solar cell in the conventional device architecture using PBDTTT-CF:PC₇₀BAAB as the active layer. A sharp contrast can be seen in the direction from the cathode to the anode. It is dark near the cathode, while bright near the anode. Because sulfur is a relatively heavy atom compared with carbon, it can strongly scatter the electrons. The domain with a high concentration of sulfur-rich PBDTTT-CF was brighter than the domain with a high concentration of carbon-rich PC₇₀BAAB in the TEM image. The results of the corresponding energy dispersive X-ray spectroscopy (EDS) are shown on the right panel of Fig. 3b. In the cross-section, the carbon content showed a decreasing trend from the cathode to the anode, while the sulfur content showed an increasing trend from the cathode to the anode and then to the poly(3,4-ethylenedioxythiophene):poly(styrenesulfonate) (PEDOT:PSS) layer. The above results confirm the vertical distribution of PC₇₀BAAB and PBDTTT-CF and that photo-polymerization induces the migration of PC₇₀BAAB through the PBDTTT-CF layer to form the VPS.

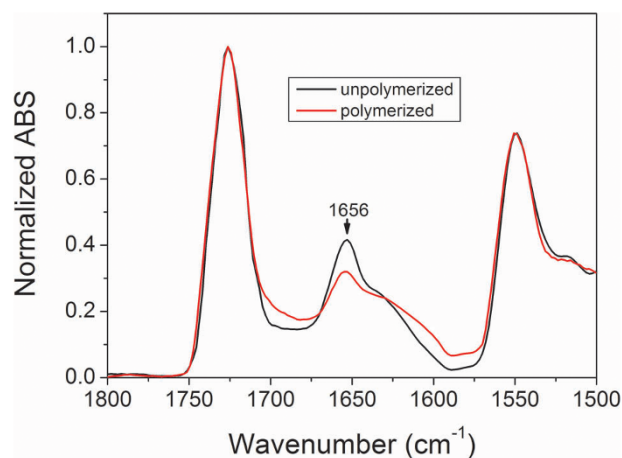


Figure 2 | FTIR spectra of the PBDTTT-CF:PC₇₀BAAB samples.

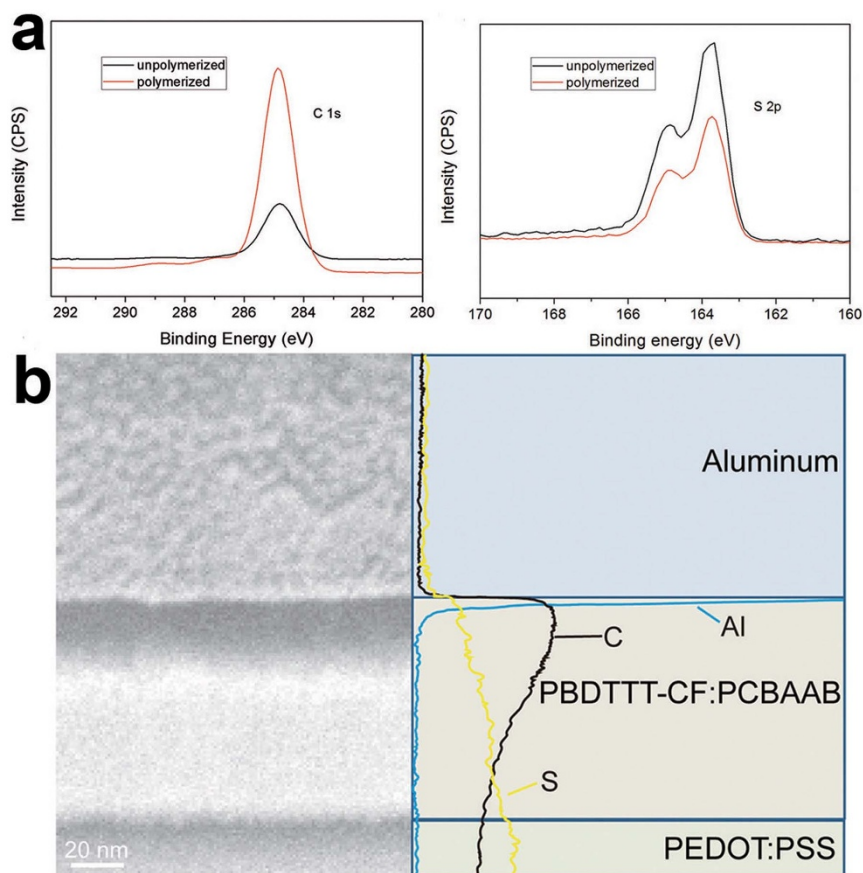


Figure 3 | (a) XPS spectra of C 1s and S 2p of the unpolymersed and polymerized samples of P3HT:PC₆₀BAAB. (b) Cross-sectional TEM image of a device using the polymerized PBDTTT-CF:PC₇₀BAAB (left), with an energy dispersive EDS scan overlaid on a schematic of the device cross-section (right).

Aggregation of donor polymer through VPS. To investigate how the vertical separation of PC₆₀BAAB affects the aggregation of the P3HT, X-ray diffraction (XRD) measurements were performed on P3HT:PC₆₀BAAB that was prepared in the standard way and subsequently polymerized (Fig. 4). The peaks at $2\theta = 5.4^\circ$ were attributed to the P3HT (100) plane, which suggests a lattice spacing of 1.64 nm. This corresponds to the interchain spacing in the P3HT which is associated with the interdigitated alkyl chains³⁸. Although the positions of the P3HT peaks remained unchanged, the peak of the polymerized sample was sharper and had a narrower full width at half maximum. This indicates that the P3HT is more crystalline in the polymerized sample. This is advantageous for hole transport.

Solar cell performance. Figure 5 shows the current density vs. voltage (J-V) characteristics of the solar cells under 100 mW/cm² air-mass 1.5 global (AM 1.5G) illumination. Device characteristics such as the short circuit current (J_{SC}), open circuit voltage (V_{OC}), fill factor (FF) and PCE are deduced from the J-V characteristics and are summarised in Table 1. The devices based on the same active layer have a similar V_{OC} because the V_{OC} of the devices is governed by the energy difference between the lowest unoccupied molecular orbital (LUMO) of the acceptor and the highest occupied molecular orbital (HOMO) of the donor, which is not affected by the polymerization of the fullerene acceptor. For the P3HT:PC₆₀BAAB-based conventional devices (see Fig. 5a), the unpolymersed device had a PCE of 2.80% with a J_{SC} of 7.67 mA/cm², a V_{OC} of 0.57 V, and a FF of 63.9%. The J_{SC} , FF and PCE of the polymerized devices improved to 9.34 mA/cm², 65.7% and 3.48%, respectively. This trend was also seen in the devices with the inverted structure. The unpolymersed device had a

PCE of 2.73% with a J_{SC} of 7.58 mA/cm², a V_{OC} of 0.57 V and a FF of 63.2%. The polymerized device had a high PCE of 3.43% with V_{OC} of 0.57 V, J_{SC} of 9.25 mA/cm² and FF of 65.5%. For the devices with the low-bandgap and high efficiency copolymer PBDTTT-CF as the donor, the polymerized devices also had a higher PCE, J_{SC} and FF, as shown in Fig. 5c and g. The device with the conventional structure based on PBDTTT-CF:PC₇₀BAAB had a PCE of 6.31% while the polymerized device demonstrates a dramatic enhancement of 24.4% and reached 7.85%. For the device with the inverted

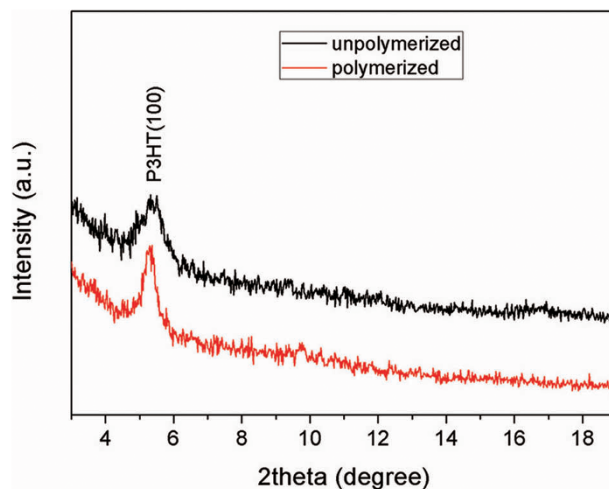


Figure 4 | X-ray diffraction patterns of the P3HT:PC₆₀BAAB sample before (black) and after (red) UV photo-polymerization.

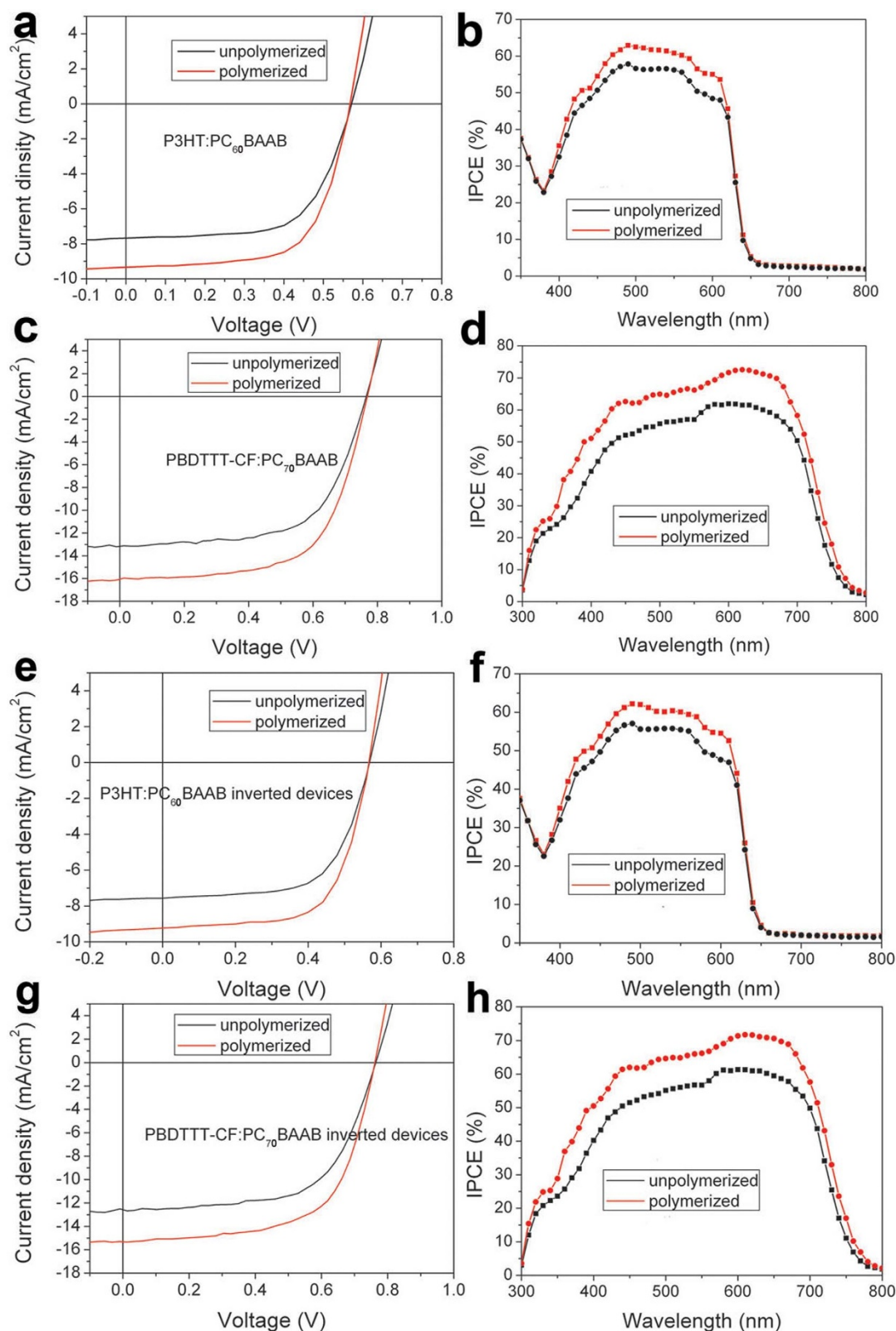


Figure 5 | Device J-V characteristics. Current density versus voltage curves (a, c, e, g) under simulated air-mass 1.5 global, AM 1.5G, radiation at 100 mW/cm² for the solar cells with either the conventional or inverted structure. The corresponding donor materials, acceptor materials and cell structures are indicated. The related incident photon to converted current efficiency (IPCE) spectra of the solar cells are shown in the right column (b, d, f, h).

structure, the situation is almost the same. To clarify the enhanced J_{SC} of the devices with VPS, we compared the incident photon to converted current efficiency spectra (IPCE, Fig. 5) of the devices with and without VPS. The IPCE results agree well with the J_{SC} of

polymer solar cells (PSCs) mentioned above. It can be concluded that for all the polymerized devices, the FF and J_{SC} increased, and so the PCE increased accordingly. These improvements are attributed to the VPS of the active layer.



Table 1 | Performance parameters of the solar cells with unpolymerized and polymerized active layers

		parameters of conventional devices				parameters of inverted devices			
		V_{OC} (V)	J_{SC} (mA/cm ²)	FF (%)	PCE (%)	V_{OC} (V)	J_{SC} (mA/cm ²)	FF (%)	PCE (%)
P3HT:PC ₆₀ BAAB	unpolymerized	0.57	7.67	63.9	2.80	0.57	7.58	63.2	2.73
	polymerized	0.57	9.34	65.7	3.48	0.57	9.25	65.5	3.43
PBDTTT-CF:PC ₇₀ BAAB	unpolymerized	0.76	13.17	62.6	6.31	0.76	12.57	62.2	5.98
	polymerized	0.76	16.06	63.6	7.85	0.76	15.32	63.1	7.37

The VPS of the donor/acceptor network also improved the charge collection efficiency under working conditions. Figure 6a shows the J - V characteristics in a wide reverse bias range under AM 1.5G illumination. The results are plotted using the net photocurrent, J_{ph} (where $J_{ph} = J_L - J_D$ and J_L and J_D are the current density under illumination and in the dark, respectively), and the dependence on the effective applied voltage, V_{eff} (where $V_{eff} = V_0 - V$ and V is the applied voltage and V_0 is the voltage at which $J_{ph} = 0$)³⁹. At a large reverse voltage ($V_{eff} > 1.5$ V), J_{ph} saturated for both devices, suggesting that all of the photogenerated excitons are dissociated into free carriers and all of the carriers are collected at the electrodes without any bimolecular recombination^{40,41}. In this case, saturation current density, J_{sat} , is only limited by the absorbed incident photo flux, N_{photon} . This means that the maximum obtainable exciton generation rates (G_{max} , given by $J_{sat} = eG_{max}L$ where L is the thickness of the active layer) are essentially the same in both devices under AM 1.5G illumination. At a slightly lower effective voltage range (0.4 V $< V_{eff} < 1.5$ V), J_{ph} - V_{eff} characteristics for both devices approach saturation and overlap with each other. Interestingly, in the low effective voltage range ($V_{eff} < 0.4$ V), J_{ph} - V_{eff} characteristics for the two devices have large differences. Because the ratio of J_{ph}/J_{sat} is essentially the product of the exciton dissociation efficiency and the charge collection efficiency⁴², a decreased J_{ph}/J_{sat} suggests either a reduced exciton dissociation efficiency or a reduced charge collection efficiency. A reduced charge collection efficiency would suggest that bimolecular recombination begins to dominate. This usually leads to lower FF⁴². The recombination in devices is manifested by the deviation of the photocurrent from the square-root dependence on the effective voltage, which is one of the signatures of recombination-limited photocurrent in organic solar cells³⁹. The superior J_{ph} - V_{eff} characteristics from the devices with VPS clearly identifies the effect of vertical phase separation on reducing the bimolecular recombination at a low effective voltage, at which maximum power output condition of PSCs usually appears.

The network with VPS was also found to prevent the build-up of space charge under device working conditions. Figure 6b and c show the experimental power law dependence of the photocurrent on the incident light intensity. A high effective voltage, V_{eff} , of 2.2 V corresponds to negative biases of -1.4 V and -1.3 V for devices with and without VPS, respectively. The power exponents are 0.93 and 0.88, respectively, which is much higher than the 0.75 exponent for the space-charge-limited scenario^{39,43}. This indicates that there was no build-up of net space charges in either devices even at the highest illumination intensity. This is because there is a high mobility of both electrons and holes with balanced mobilities. However, at a low effective voltage of 0.2 V, which corresponds to an external bias of 0.7 V for devices without VPS, the power exponent decreased to 0.84 (Fig. 5c). This implies a build-up of space charge and subsequent bimolecular recombination⁴³. In contrast, the power exponent for devices with vertical phase separation remained 0.93 at $V_{eff} = 0.2$ V, corresponding to an external bias of 0.6 V (Fig. 6b) which indicates that there was no space charge build-up. The results clearly show that VPS effectively prevents space charge build-up even under low effective voltages, which is usually at the maximum power output of PSCs.

It can be concluded that the VPS of the donor and the acceptor was induced by UV photo-polymerization of the acceptor in BHJ structure, similar to the introduction of some solvent additives which affect the morphology and the charge carrier transport and recombination⁴⁴. This effectively reduced the build-up of space charge and the subsequent bimolecular recombination, which improved the charge collection ability, resulting in the enhanced FF and J_{SC} .

In addition, to confirm that there was a more continuous charge transport channel which reduced the charge accumulation in the devices fabricated using photo-polymerization, the P3HT:PC₆₀BAAB device was illuminated continuously under simulated air-mass 1.5 global, AM 1.5G radiation at 100 mW/cm². The corresponding J_{SC} was obtained every 30 s. As shown in Fig. 7, the J_{SC} of the

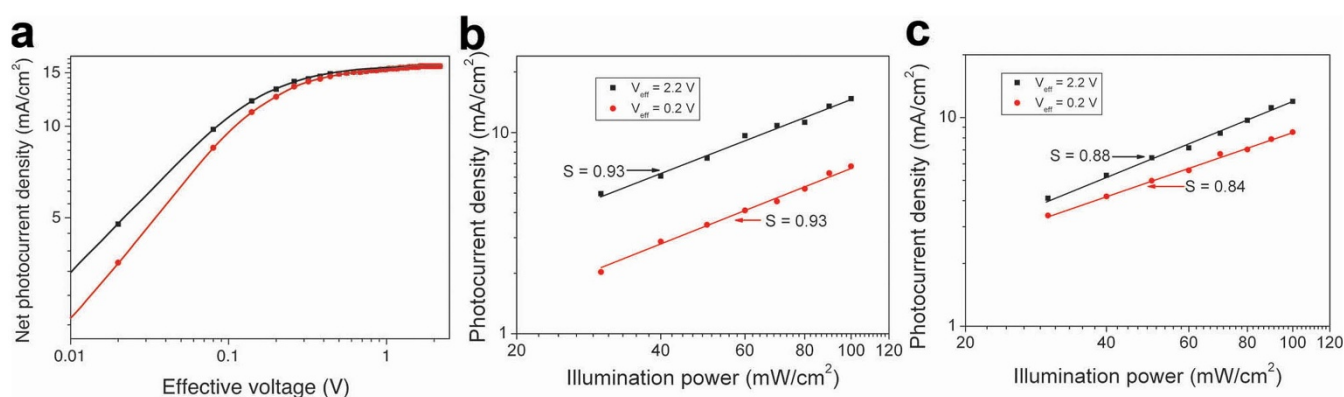


Figure 6 | (a) Photocurrent density versus effective voltage (J_{ph} - V_{eff}) characteristics of a PBDTTT-CF:PC₇₀BAAB solar cell that has a conventional device architecture with (black) and without (red) VPS structure under constant incident light intensity (AM 1.5G, 100 mW/cm²). The current from device that has VPS with the conventional device architecture has a dependence on the intensity of the incident light. A double logarithmic plot of the photocurrent density as a function of the incident light intensity for the PBDTTT-CF:PC₇₀BAAB solar cells with (b) and without (c) VPS with different effective voltages is also shown.

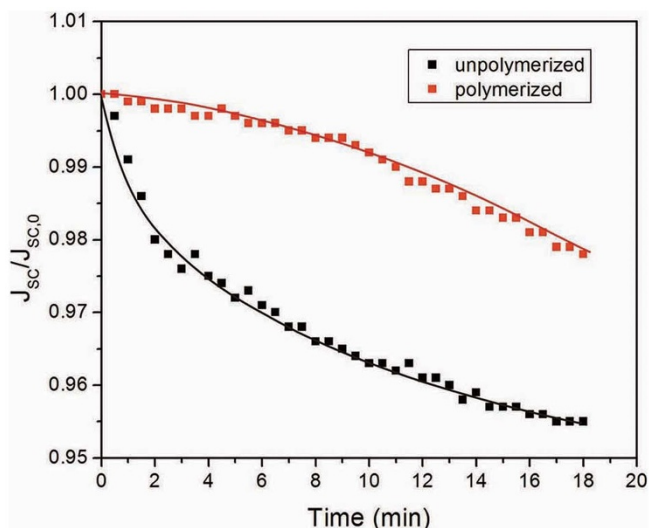


Figure 7 | Relationship between the short circuit current and the illumination time for P3HT:PC₆₀BAAB devices, fabricated without (black) and with (red) UV induced photo-polymerization. $J_{sc,0}$ is the initial J_{sc} .

unpolymerized device decreased quickly under illumination, while that of the polymerized device decreased slowly. As mentioned above, the conventional acceptor fullerene, PCBM, forms a discontinuous island structure, resulting in a more discontinuous island structure of the unpolymerized device. Therefore, more charge accumulated and could not be transported to the electrodes, leading to a decreased J_{sc} . The polymerized device, having a more continuous structure induced by the photo-polymerization of the PCBAAB prevented charge accumulation, and so the J_{sc} slowly decreased with extended illumination. Therefore, VPS induced by the photo-polymerization of the fulleride is an effective method for forming a continuous network that can decrease the charge accumulation.

To further verify the applicability of photo-polymerization induced VPS of the donor and the acceptor to improve the device performance, the donor polymer was covalently bound to the anode via self-assembly to reduce the energy barrier. This improved the carrier extraction ability as shown in our previous work³⁷. The PCE of the device with photo-polymerization induced VPS reached 8.47%. This is an enhancement of 34% compared with the device with PEDOT:PSS buffer layer and without photo-polymerization induced VPS. The device J-V characteristics are shown in Fig. 8.

Discussion

Although many methods to achieve VPS have been developed, there is not a universal method which is applicable to any donor-acceptor system. Here, we introduce the photo-polymerized acrylate group to the fullerene acceptor, and used the relative migration of the donor and the acceptor during polymerization to achieve real VPS. We believe that this method is universal and controllable because the fullerene is by far the most common acceptor. Also, the relative migration of the donor and the acceptor were controlled by adjusting the intensity of the UV light.

UV photo-polymerization of the fulleride acceptor formed a more continuous structure of the acceptor as well as VPS of the donor and the acceptor. The VPS in the BHJ device architecture effectively reduces the build-up of space charge and subsequent bimolecular recombination. This improves the charge collection ability of the device, resulting in the improved FF and J_{sc} , which improved the PCE. The more continuous network formed by UV photo-polymerization aids charge carrier transport. This reduces the charge accumulation in the device and so there is less degradation of the device

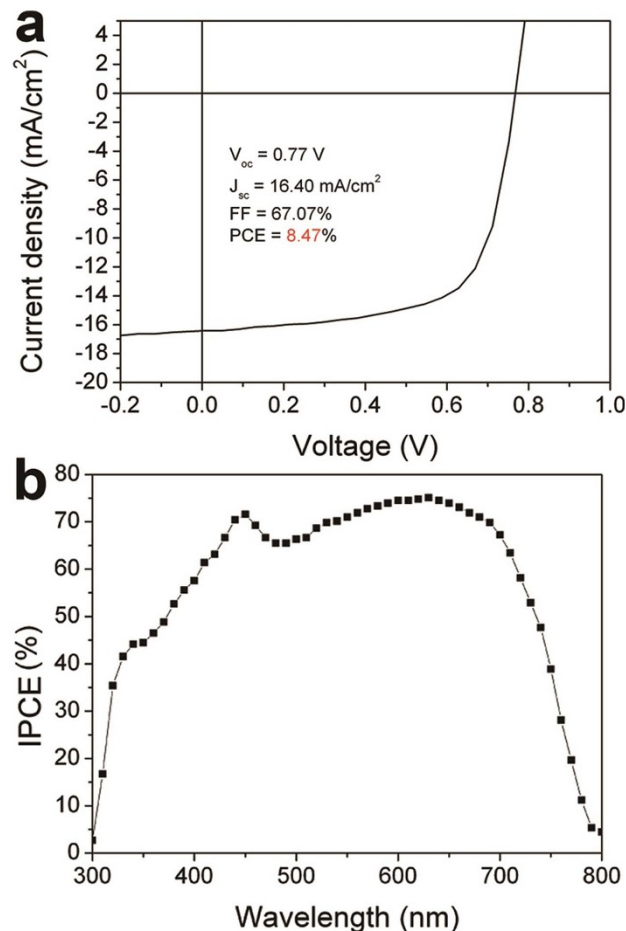


Figure 8 | J-V characteristics from a device. (a) The current density versus voltage curves (under simulated air-mass 1.5 global, AM 1.5G, radiation at 100 mW/cm²) for the solar cells with the donor polymer covalently bound to the anode as well as the photo-polymerization induced VPS structure. (b) The related IPCE spectra of the solar cell.

performance as the illumination time increased compared with the devices which did not have VPS. The UV polymerization of the fulleride acceptor, regardless of whether the donor material is a polymer or a small organic molecule, forms a more continuous structure as well as VPS. This is a general method that provides a novel approach to control the morphology of the active layer not only for conventional, but also for inverted device architectures.

Methods

Materials. PC₆₀BM and PC₇₀BM were purchased from Solenne B V. P3HT was purchased from Rieke Metals. PBDTTT-CF was purchased from 1-Material. All the materials were used as received.

Synthesis and characterization. PC₆₀BAAB was synthesised using the esterification of 4-hydroxybutyl acrylate and [6,6]-phenyl-C61-butyric acid (PC₆₀BA). The PC₆₀BA was prepared from the hydrolysis of PC₆₀BM⁴⁵, using *N*-(3-Dimethylaminopropyl)-*N'*-ethylcarbodiimide hydrochloride (EDC) as the coupling agent and 4-(dimethylamino)pyridine (DMAP) as the catalyst. PC₇₀BAAB was synthesised using the same procedure.

¹H NMR spectra were recorded using Bruker DRX-500 spectrometers.

PC₆₀BAAB. ¹H NMR (CDCl₃, 500 MHz): δ 1.86–1.87 (d, 4H), 2.18–2.24 (m, 2H), 2.52–2.55 (m, 2H), 2.90–2.95 (m, 2H), 4.24–4.26 (d, 2H), 4.32–4.34 (d, 2H), 5.83–5.86 (d, 1H), 6.09–6.18 (m, 1H), 6.40–6.45 (d, 1H), 7.48–7.50 (m, 1H), 7.55–7.58 (m, 2H), 7.93–7.96 (m, 2H).

PC₇₀BAAB. ¹H NMR (CDCl₃, 500 MHz): δ 1.85–1.86 (d, 4H), 2.17–2.23 (m, 2H), 2.51–2.54 (m, 2H), 2.88–2.94 (m, 2H), 4.22–4.25 (d, 2H), 4.31–4.33 (d, 2H), 5.81–5.83 (d, 1H), 6.07–6.18 (m, 1H), 6.39–6.44 (d, 1H), 7.48–7.51 (m, 1H), 7.56–7.58 (m, 2H), 7.94–7.96 (m, 2H).



Device fabrication and characterization. Unless otherwise specified, all processes were performed in the air. The conventional photovoltaic cells were fabricated by spin-casting the active bulk heterojunction layer onto a 30 nm layer of PEDOT:PSS (H. C. Stark Baytron) on liquid-crystal-display glass patterned with 120 nm of indium tin oxide (ITO). All solutions were prepared by dissolving the corresponding donor and acceptor into dichlorobenzene. For P3HT:PC₆₀BAAB, a ratio of 1 : 1 w/w was used with a total polymer concentration of 20 mg/mL. For the other systems, a ratio of 1 : 1.5 w/w was used with a total polymer concentration of 10 mg/mL. The solutions also had a 3% volume ratio of the additive 1,8-diiodooctane. For the P3HT:PC₆₀BAAB blend, the active layer was 150 nm thick, while for the other system, the thickness was 100 nm. LiF (0.5 nm) and Al (100 nm) were deposited through a shadow mask by thermal evaporation under a vacuum pressure of $\sim 5 \times 10^{-4}$ Pa. The device had a diameter of 2 mm. To form the polymerized films, the spin-cast samples were transferred to a covered glass petri dish and irradiated with 365 nm UV light at an intensity of 0.1 mW/cm² under N₂ for 40 min.

The active layers of the inverted photovoltaic cells were the same as the conventional ones. The difference was that the ITO glass was modified with 80% ethoxylated polyethylenimine, to reduce the work function⁴⁶. In addition, 15 nm of MoO₃ as an anode buffer layer and 150 nm of Ag as the anode were deposited under a vacuum pressure of $\sim 5 \times 10^{-4}$ Pa.

Current density-voltage (J-V) curves were measured using a Keithley 2611 power source meter under AM 1.5G illumination (100 mW/cm²) using a 300 W Newport-Oriel AM 1.5G light source. All measurements were carried out in air. The devices were not encapsulated.

FTIR spectra were obtained by using a Bruker Vector 22 at 4 cm⁻¹ resolution with 64 scans performed at ambient temperature. Samples were prepared by immersing the film on PEDOT:PSS coated ITO substrates in deionised water and picking up the floating active layer with 200 mesh Cu grids. The active layers were tableted with KBr after drying. The XPS measurements were performed on an AXIS-Ultra instrument from Kratos Analytical using monochromatic Al K α radiation (225 W, 15 mA, 15 kV) and low-energy electron flooding for charge compensation. To compensate for surface charge effects, binding energies were calibrated using the hydrocarbon C 1s peak at 284.80 eV. The data were converted into VAMAS file format and imported into the CasaXPS software package for analysis. The X-ray measurements were carried out on a Bruker D8 Advance powder diffractometer equipped with a Cu anode (λ K α_1 = 0.154056 nm). A Focused Ion Beam (FIB) system (FEI Nova 200 Nanolab) was used to prepare cross-sections of the device by *in situ* lift-out. The cutting was performed using 30 kV Ga⁺ ions. A JEOL 2010 FEG analytical electron microscope operated at 200 kV was used to obtain transmission electron microscope images. Energy-dispersive X-ray spectroscopy (EDS) spectra were obtained from the TEM samples.

- Oosterhout, S. D. *et al.* The effect of three-dimensional morphology on the efficiency of hybrid polymer solar cells. *Nat. Mater.* **8**, 818–824 (2009).
- Lee, J. K. *et al.* Processing additives for improved efficiency from bulk heterojunction solar cells. *J. Am. Chem. Soc.* **130**, 3619–3623 (2008).
- Haugeneder, A. *et al.* Exciton diffusion and dissociation in conjugated polymer/fullerene blends and heterostructures. *Phys. Rev. B: Condens. Matter* **59**, 15346–15351 (1999).
- Hau, S. K., Yip, H.-L., Chen, K.-S., Zou, J. & Jen, A. K. Y. Solution processed inverted tandem polymer solar cells with self-assembled monolayer modified interfacial layers. *Appl. Phys. Lett.* **97**, 253307 (2010).
- Yu, G., Gao, J., Hummelen, J. C., Wudl, F. & Heeger, A. J. Polymer photovoltaic cells: enhanced efficiencies via a network of internal donor-acceptor heterojunctions. *Science* **270**, 1789–1791 (1995).
- Halls, J. J. M. *et al.* Efficient photodiodes from interpenetrating polymer networks. *Nature* **376**, 498–500 (1995).
- Shaheen, S. E. *et al.* 2.5% efficient organic plastic solar cells. *Appl. Phys. Lett.* **78**, 841–843 (2001).
- Yang, X. *et al.* Nanoscale morphology of high-performance polymer solar cells. *Nano Lett.* **5**, 579–583 (2005).
- Yang, X. & Loos, J. Toward high-performance polymer solar cells: the importance of morphology control. *Macromolecules* **40**, 1353–1362 (2007).
- Müller, C. *et al.* Binary organic photovoltaic blends: a simple rationale for optimum compositions. *Adv. Mater.* **20**, 3510–3515 (2008).
- Cheyns, D., Gommans, H., Odijk, M., Genoe, J. & Heremans, P. Stacked organic solar cells based on pentacene and C₆₀. *Sol. Energy Mater. Sol. Cells* **91**, 399–404 (2007).
- Colson, A., Junge, J., Kayser, C. & Lemmer, U. Organic tandem solar cells comprising polymer and small-molecule subcells. *Appl. Phys. Lett.* **89**, 203506 (2006).
- Sista, S. *et al.* Highly efficient tandem polymer photovoltaic cells. *Adv. Mater.* **22**, 380–383 (2010).
- Ma, W., Yang, C., Gong, X., Lee, K. & Heeger, A. J. Thermally stable, efficient polymer solar cells with nanoscale control of the interpenetrating network morphology. *Adv. Funct. Mater.* **15**, 1617–1622 (2005).
- Xu, Z. *et al.* Vertical phase separation in poly(3-hexylthiophene): fullerene derivative blends and its advantage for inverted structure solar cells. *Adv. Funct. Mater.* **19**, 1227–1234 (2009).
- Kim, Y. *et al.* Device annealing effect in organic solar cells with blends of regioregular poly(3-hexylthiophene) and soluble fullerene. *Appl. Phys. Lett.* **86**, 063502 (2005).
- Chen, L.-M., Xu, Z., Hong, Z. & Yang, Y. Interface investigation and engineering-achieving high performance polymer photovoltaic devices. *J. Mater. Chem.* **20**, 2575–2598 (2010).
- Chen, L.-M., Hong, Z., Li, G. & Yang, Y. Recent progress in polymer solar cells: manipulation of polymer:fullerene morphology and the formation of efficient inverted polymer solar cells. *Adv. Mater.* **21**, 1434–1449 (2009).
- Huang, Y.-C., Welch, G. C., Bazan, G. C., Chabinyc, M. L. & Su, W.-F. Self-vertical phase separation study of nanoparticle/polymer solar cells by introducing fluorinated small molecules. *Chem. Commun.* **48**, 7250–7252 (2012).
- Xue, B. *et al.* Vertical stratification and interfacial structure in P3HT:PCBM organic solar cells. *J. Phys. Chem. C* **114**, 15797–15805 (2010).
- Wei, H. X. *et al.* Thermal annealing-induced vertical phase separation of copper phthalocyanine:fullerene bulk heterojunction in organic photovoltaic cells. *Appl. Phys. Lett.* **97**, 083302 (2010).
- Jouane, Y. *et al.* Annealing treatment for restoring and controlling the interface morphology of organic photovoltaic cells with interfacial sputtered ZnO films on P3HT:PCBM active layers. *J. Mater. Chem.* **22**, 1606–1612 (2012).
- Cheun, H. *et al.* Roles of thermally-induced vertical phase segregation and crystallization on the photovoltaic performance of bulk heterojunction inverted polymer solar cells. *Energy Environ. Sci.* **4**, 3456–3460 (2011).
- Karagiannidis, P. G., Georgiou, D., Pitsalidis, C., Laskarakis, A. & Logothetidis, S. Evolution of vertical phase separation in P3HT:PCBM thin films induced by thermal annealing. *Mater. Chem. Phys.* **129**, 1207–1213 (2011).
- Kokubu, R. & Yang, Y. Vertical phase separation of conjugated polymer and fullerene bulk heterojunction films induced by high pressure carbon dioxide treatment at ambient temperature. *Phys. Chem. Chem. Phys.* **14**, 8313–8318 (2012).
- Song, T., Wu, Z., Tu, Y., Jin, Y. & Sun, B. Vertical phase segregation of hybrid poly(3-hexylthiophene) and fullerene derivative composites controlled via velocity of solvent drying. *Semicond. Sci. Technol.* **26**, 034009-1–034009-7 (2011).
- Ruderer, M. A. *et al.* Solvent-induced morphology in polymer-based systems for organic photovoltaics. *Adv. Funct. Mater.* **21**, 3382–3391 (2011).
- Susarova, D. K., Troshin, P. A., Moskvin, Y. L., Babenko, S. D. & Razumov, V. F. Vertical concentration gradients in bulk heterojunction solar cells induced by differential material solubility. *Thin Solid Films* **519**, 4132–4135 (2011).
- Anselmo, A. S. *et al.* Tuning the vertical phase separation in polyfluorene:fullerene blend films by polymer functionalization. *Chem. Mater.* **23**, 2295–2302 (2011).
- Li, H. *et al.* Solvent-soaking treatment induced morphology evolution in P3HT/PCBM composite films. *J. Mater. Chem.* **21**, 6563–6568 (2011).
- Yuan, D. *et al.* The improvement of bulk-heterojunction order in polymer photovoltaic device. *Spectrosc. Spect. Anal.* **31**, 3175–3179 (2011).
- Chien, S.-C., Chen, F.-C., Chung, M.-K. & Hsu, C.-S. Self-assembled poly(ethylene glycol) buffer layers in polymer solar cells: toward superior stability and efficiency. *J. Phys. Chem. C* **116**, 1354–1360 (2012).
- Liu, Z. *et al.* High-efficiency hybrid solar cells based on polymer/PbS₂Se_{1-x} nanocrystals benefiting from vertical phase segregation. *Adv. Mater.* **25**, 5772–5778 (2013).
- Broer, D. J., Lub, J. & Mol, G. N. Wide-band reflective polarizers from cholesteric polymer networks with a pitch gradient. *Nature* **378**, 467–469 (1995).
- Hikmet, R. A. M. & Kemperman, H. Electrically switchable mirrors and optical components made from liquid-crystal gels. *Nature* **392**, 476–479 (1998).
- Broer, D. J., Mol, G. N., van Haaren, J. A. M. M. & Lub, J. Photo-induced diffusion in polymerizing chiral-nematic media. *Adv. Mater.* **11**, 573–578 (1999).
- Zhang, L. *et al.* Highly efficient polymer solar cells by using the homogeneous self-assembly of a sulphhydryl-capped photoactive polymer covalently bound to the anode. *Energy Tech.* **1**, 613–616 (2013).
- Lee, J. U., Kim, Y. D., Jo, J. W., Kim, J. P. & Jo, W. H. Efficiency enhancement of P3HT/PCBM bulk heterojunction solar cells by attaching zinc phthalocyanine to the chain-end of P3HT. *J. Mater. Chem.* **21**, 17209–17218 (2011).
- Mihailetchi, V. D., Wildeman, J. & Blom, P. W. M. Space-charge limited photocurrent. *Phys. Rev. Lett.* **94**, 126602 (2005).
- Blom, P. W. M., Mihailetchi, V. D., Koster, L. J. A. & Markov, D. E. Device physics of polymer:fullerene bulk heterojunction solar cells. *Adv. Mater.* **19**, 1551–1566 (2007).
- Peet, J. *et al.* Efficiency enhancement in low-bandgap polymer solar cells by processing with alkane dithiols. *Nat. Mater.* **6**, 497–500 (2007).
- Mihailetchi, V. D., Koster, L. J. A., Hummelen, J. C. & Blom, P. W. M. Photocurrent generation in polymer-fullerene bulk heterojunctions. *Phys. Rev. Lett.* **93**, 216601 (2004).
- Lenes, M., Morana, M., Brabec, C. J. & Blom, P. W. M. Recombination-limited photocurrents in low bandgap polymer/fullerene solar cells. *Adv. Funct. Mater.* **19**, 1106–1111 (2009).
- Venkatesan, S. *et al.* Interplay of nanoscale domain purity and size on charge transport and recombination dynamics in polymer solar cells. *Nanoscale* **6**, 1011–1019 (2014).
- Wei, Q., Tajima, K., Tong, Y., Ye, S. & Hashimoto, K. Surface-segregated monolayers: a new type of ordered monolayer for surface modification of organic semiconductors. *J. Am. Chem. Soc.* **131**, 17597–17604 (2009).



46. Zhou, Y. *et al.* A universal method to produce low-work function electrodes for organic electronics. *Science* **336**, 327–332 (2012).

Acknowledgments

This study was financially supported by the NSFC (Grants 10934001, 61177020, and 11121091) and the National Basic Research Program of China (2009CB930504, 2013CB328704).

Author contributions

L.Z. carried out the experimental work with the assistance of X.X. and L.Z. on some of the experiments. Z.C., L.X. and Q.G. guided the work and the analysis. L.Z., Z.C., L.X. and B.Q. wrote the paper.

Additional information

Competing financial interests: The authors declare no competing financial interests.

How to cite this article: Zhang, L.P. *et al.* Vertical phase separation in bulk heterojunction solar cells formed by *in situ* polymerization of fulleride. *Sci. Rep.* **4**, 5071; DOI:10.1038/srep05071 (2014).



This work is licensed under a Creative Commons Attribution-NonCommercial-NoDerivs 3.0 Unported License. The images in this article are included in the article's Creative Commons license, unless indicated otherwise in the image credit; if the image is not included under the Creative Commons license, users will need to obtain permission from the license holder in order to reproduce the image. To view a copy of this license, visit <http://creativecommons.org/licenses/by-nc-nd/3.0/>